Molecular Therapy
Oncolytics
Original Article

Route of 41BB/41BBL Costimulation Determines Effector Function of B7-H3-CAR.CD28ζ T Cells

Phuong Nguyen,[1] Emmanuel Okeke,[1] Michael Clay,[2] Dalia Haydar,[1] Julie Justice,[2] Carla O'Reilly,[1] Shondra Pruett-Miller,[3] James Papizan,[3] Jennifer Moore,[1] Sheng Zhou,[4] Robert Throm,[5] Giedre Krenciute,[1] Stephen Gottschalk,[1] and Christopher DeRenzo[1]

[1]Department of Bone Marrow Transplantation and Cellular Therapy, St. Jude Children's Research Hospital, Memphis, TN 38105, USA; [2]Department of Pathology, St. Jude Children's Research Hospital, Memphis, TN 38105, USA; [3]Department of Cell and Molecular Biology, St. Jude Children's Research Hospital, Memphis, TN 38105, USA; [4]Experimental Cellular Therapeutics Laboratory, St. Jude Children's Research Hospital, Memphis, TN 38105, USA; [5]Vector Development and Production Laboratory, St. Jude Children's Research Hospital, Memphis, TN 38105, USA

B7-H3 is actively being explored as an immunotherapy target for pediatric patients with solid tumors using monoclonal antibodies or T cells expressing chimeric antigen receptors (CARs). B7-H3-CARs containing a 41BB costimulatory domain are currently favored by several groups based on preclinical studies. In this study, we initially performed a detailed analysis of T cells expressing B7-H3-CARs with different hinge/transmembrane (CD8α versus CD28) and CD28 or 41BB costimulatory domains (CD8α/CD28, CD8α/41BB, CD28/CD28, CD28/41BB). Only subtle differences in effector function were observed between CAR T cell populations *in vitro*. However, CD8α/CD28-CAR T cells consistently outperformed other CAR T cell populations in three animal models, resulting in a significant survival advantage. We next explored whether adding 41BB signaling to CD8α/CD28-CAR T cells would further enhance effector function. Surprisingly, incorporating 41BB signaling into the CAR endodomain had detrimental effects, while expressing 41BBL on the surface of CD8α/CD28-CAR T cells enhanced their ability to kill tumor cells in repeat stimulation assays. Furthermore, 41BBL expression enhanced CD8α/CD28-CAR T cell expansion *in vivo* and improved antitumor activity in one of four evaluated models. Thus, our study highlights the intricate interplay between CAR hinge/transmembrane and costimulatory domains. Based on our study, we selected CD8α/CD28-CAR T cells expressing 41BBL for early phase clinical testing.

INTRODUCTION

Solid tumors contribute disproportionately to the morbidity and mortality of all pediatric patients with cancer despite aggressive management with multimodality therapy.[1] This problem is especially acute in children and young adults with relapsed or refractory disease,[2–6] whose poor rates of survival have remained relatively unchanged during the last two decades.[1] Thus, new therapeutic strategies are needed to improve outcomes and reduce treatment-related complications for this group of patients. Treatment with chimeric antigen receptor (CAR) T cells offers a promising approach to enhance survival without the overlapping toxicities observed with conventional chemotherapy.

Individual pediatric solid tumor types are rare, and thus developing CAR T cells to recognize one antigen found on multiple solid tumors is ideal. B7-H3 (CD276) is a transmembrane glycoprotein expressed in a high percentage of solid tumors with limited expression in normal tissues.[7–10] B7-H3 is part of the B7-CD28 immune modulatory family,[11] and it functions to inhibit T cell activation and proliferation.[12] B7-H3-CAR T cells targeting solid tumors have been described, and they exhibit antitumor activity without reported toxicity in murine models.[10,13–15] However, most evaluated B7-H3-CARs follow a second-generation (2G) design, incorporating either CD28 or 41BB costimulatory (costim) domains. Since 2G-CAR T cells targeting other solid tumor antigens, including HER2 and mesothelin, have limited antitumor activity in early-phase clinical studies,[16,17] there is concern that 2G-CAR T cells targeting B7-H3 will have limited antitumor activity in humans.

Several approaches are currently being pursued to increase the antitumor activity of 2G-CAR T cells, including the transgenic expression of cytokines, chimeric cytokine receptors, or knocking out genes that inhibit T cell function.[18–20] Another approach is to provide additional costimulation to 2G-CAR T cells, either by incorporating additional costim domains to generate third-generation (3G) CARs,[21] or expressing ligands of costim molecules on their cell surface.[22] While studies focused on CD19-CAR T cells have demonstrated that expression of 41BB ligand (41BBL) on the surface of CD28.ζ CAR T cells is superior to incorporating 41BB signaling into the CD28.ζ CAR endodomain,[23] this has not been evaluated for other 2G CARs.

To explore how to best provide CD28 and 41BB costimulation to T cells expressing B7-H3-CARs, we first compared the effector function of four 2G CARs with different hinge/transmembrane (H/TM)

Received 14 February 2020; accepted 19 June 2020;
https://doi.org/10.1016/j.omto.2020.06.018.

Correspondence: Christopher DeRenzo, Department of Bone Marrow Transplantation and Cellular Therapy, St. Jude Children's Research Hospital 262 Danny Thomas Place, MS 310, Memphis, TN 38105, USA.
E-mail: chris.derenzo@stjude.org

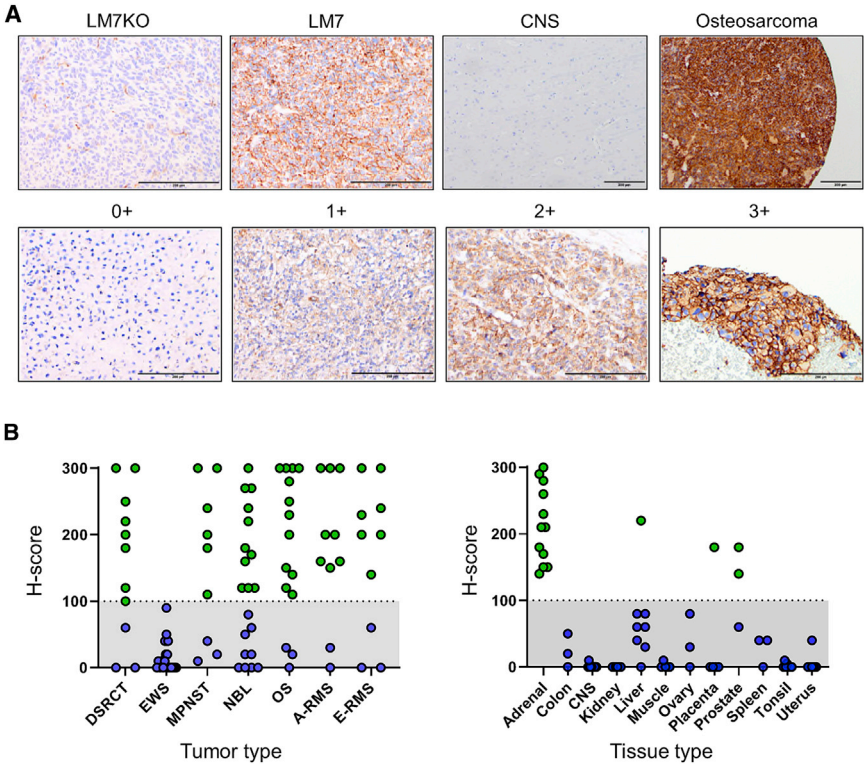

Figure 1. IHC for B7-H3 on Pediatric Solid Tumors and Normal Adult Tissues

Pediatric solid tumors and normal tissues were evaluated for B7-H3 expression by IHC. (A) Representative images for LM7KO (B7-H3$^{-/-}$) and LM7 (B7-H3$^{+/+}$) tumors, CNS tissue, and osteosarcoma. Staining intensity: 0^{+}, no staining; 1^{+}, weak positive; 2^{+}, moderate positive; 3^{+}, strong positive. Scale bars represent 200 μm. (B) H-scores for pediatric solid tumors (left panel) and normal tissues (right panel).

and CD28 or 41BB costim domains. We then evaluated the best strategy to combine both signals. From our detailed 2G CAR comparison, one of the two designed CD28.ζ CARs emerged as the lead CAR. Incorporating the 41BB signaling domain into this CAR had detrimental effects on CAR T cell function, whereas 41BBL surface expression significantly enhanced effector function.

RESULTS

Pediatric Solid Tumors Express B7-H3

We evaluated B7-H3 protein expression in tumor and normal tissue by performing immunohistochemistry (IHC) on formalin-fixed, paraffin-embedded sections from pediatric solid tumor and adult normal tissue microarrays (TMAs). To establish positive and negative controls, we inoculated NSG mice with B7-H3$^{+/+}$ LM7 or B7-H3$^{-/-}$ LM7 (LM7 knockout [KO]) cells, followed by tumor harvest, sectioning, and staining. LM7 tumors grown *in vivo* were diffusely B7-H3-positive, while LM7KO tumors had only minimal background staining, confirming specificity of the B7-H3 antibody (Figure 1A). Using an H-score ≥100 to determine positive versus negative samples, we found that a high percentage of pediatric solid tumors were B7-H3-positive (Figure 1B), including desmoplastic small round cell tumor (DSRCT) (73%), malignant peripheral nerve sheath tumor (MPNST) (67%), neuroblastoma (NBL) (55%), osteosarcoma (OS) (80%), alveolar rhabdomyosarcoma (80%), and embryonal rhabdomyosarcoma (70%). All Ewing sarcoma (EWS) tumors evaluated were negative (N = 20). For normal tissues, the majority were completely B7-H3-negative or had an H-score less than 100 (Figure 1B; Figure S1), except for adrenal cortex (H-score 300, N = 1) and adrenal medulla (H-score 170, N = 1). To further evaluate B7-H3 expression on adrenal tissue, we stained pediatric whole-section non-neoplastic adrenal glands and 10/10 were positive.

Generation of B7-H3-CAR T Cells

Four lentiviral vectors (LVs) were generated encoding 2G B7-H3-CARs utilizing a single-chain variable fragment (scFv) derived from the humanized B7-H3-specific monoclonal antibody (mAb) MGA271,[8] CD3ζ, and combinations of two different H/TM (CD8α or CD28) and costim (CD28 or 41BB) domains (CD8α/CD28, CD8α/41BB, CD28/CD28, CD28/41BB) (Figure 2A; Figure S2). T cells transduced with a non-functional B7-H3-CAR containing a CD8α H/TM domain without a signaling domain served as control (CD8α/Δ). Healthy donor-activated T cells were transduced with LVs at a multiplicity of infection (MOI) of 50. Transduction efficiency was determined by measuring vector copy number (VCN) and CAR surface expression. All constructs successfully transduced human T cells (Figures 2B–2D, black asterisks: N = 13, $p < 0.001$). LVs encoding the CD28/CD28 CARs had significantly lower transduction as judged by VCN (N = 13, $p < 0.01$), resulting in a lower cell surface expression of CARs (N = 13, $p < 0.001$) compared to all other 2G constructs (Figures 2C and 2D; blue asterisks). Phenotyping of CAR-positive cells demonstrated comparable CD4- to CD8-positive T cell ratios, as well as T cell memory phenotypes for the 2G CARs (Figures 2E and 2F). In summary, 2G B7-H3-CAR LV constructs successfully transduced human T cells with comparable phenotype. However, transduction efficiency was consistently lowest for CD28/CD28-CARs.

CD28-CAR T Cells Have Superior Effector Function *In Vitro*

To evaluate expansion and basal apoptosis, T cells were grown in media containing interleukin 7 (IL-7)/IL-15 and quantified on day 9 or 10 post-transduction to measure overall fold expansion, and stained with annexin V and DAPI to measure the percentage of apoptotic cells. 2G CARs with a CD28 costim domain had greater expansion compared to those with a 41BB costim domain (Figure 3A; N = 10, $p < 0.05$). There was no difference in expansion when comparing

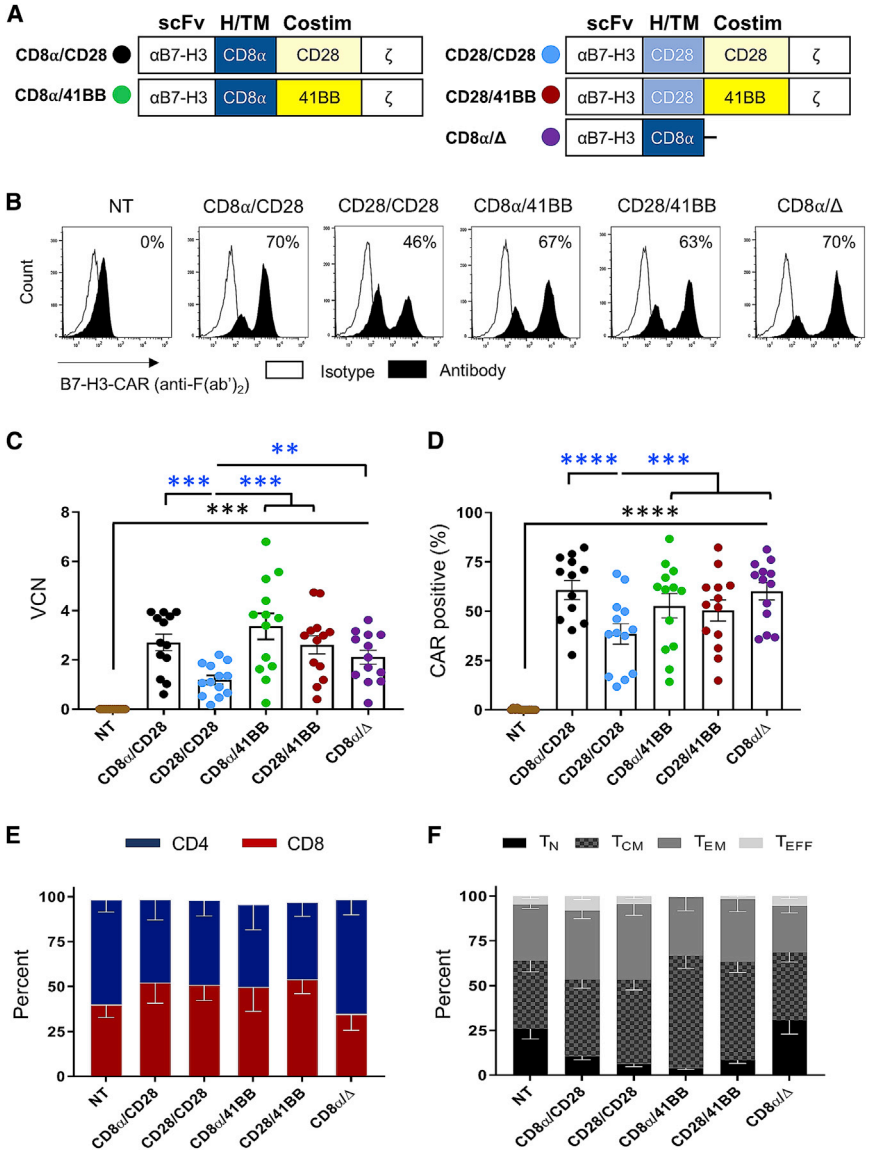

Figure 2. Transduction and Phenotypes of 2G B7-H3-CAR T Cells

Activated T cells were transduced with LV particles encoding 2G B7-H3-CARs or a control CAR (CD8α/Δ). Vector copy number (VCN) was determined by digital droplet PCR. CAR surface expression was measured by flow cytometry. (A) Schematic representation of 2G CAR LVs. The color in the circle is used throughout to identify constructs. (B) Representative flow plots of non-transduced (NT) and transduced T cells. (C and D) VCN (C) and CAR (D) surface expression (N = 13; one-way ANOVA; black asterisks, comparison to NT T cells; blue asterisks, comparison between 2G CARs). (E and F) CD4/CD8 ratios (E) and memory phenotypes (F) (N = 5). Data, mean ± SEM. **p < 0.01, ***p < 0.001, ****p < 0.0001.

non-transduced (NT) T cells, CD8α/CD28, CD28/CD28, or CD8α/Δ, or comparing CD8α/41BB to CD28/41BB. 2G CARs with a 41BB costim domain had greater basal apoptosis compared to NT T cells (Figure 3B; N = 8, p < 0.05), whereas no significant difference was found when comparing CD8α/CD28, CD28/CD28, or CD8α/Δ to NT T cells.

To evaluate 2G CAR T cell specificity and cytokine production we used tumor cells for which we confirmed absence (LM7KO) or presence of B7-H3 (LM7, A549, U373) by flow cytometry (Figure S3). T cells were incubated with tumor cells, and after 24 h supernatants were collected for quantitative ELISA to measure interferon γ (IFNγ) and IL-2. All functional 2G B7-H3-CARs specifically recognized B7-H3-positive targets as judged by greater IFNγ production in the presence of B7-H3-positive (LM7) compared to B7-H3-negative (LM7KO) tumor cells (Figure 3C; blue asterisks, N = 4, p < 0.01). In addition, high levels of IFNγ production were observed in the presence of the other two (A549, U373) B7-H3-positive tumor cells. While 2G CARs with a CD28 costim domain or controls induced minimal IFNγ in the absence of B7-H3 antigen (media or LM7KO), 2G CARs with a 41BB endodomain induced significant IFNγ production in comparison to controls without antigenic stimulation (media only or LM7KO), indicative for tonic signaling (Figure 3C; red asterisks, N = 4, p < 0.01). Furthermore, 2G CARs with 41BB costim domains secreted limited amounts of IL-2 in comparison to 2G CARs with CD28 costim domains in the presence of B7-H3-positive tumors (Figure 3D; black asterisks, N = 4, p < 0.05).

To characterize *in vitro* antitumor activity, an impedance assay (xCELLigence) was used to determine killing of B7-H3-positive tumors (LM7). Cells were cocultured at a 0.5 T cell-to-1 tumor cell ratio without exogenous cytokines. Seventy-two hours post-incubation, cytolysis was measured and T cells were plated on fresh tumors for repeat stimulation. The assay was repeated for each donor until no CAR T cell population killed >50% of tumor cells. Given that donor variability affects CAR T cell repeat killing capacity, the last stimulation where CAR T cells killed >50% of targets was deemed the final stimulation for each donor. Figure S4 shows individual stimulations for all donors tested, and Figures 3E and 3F show summary data. After the first stimulation, all 2G CARs killed ~100% of targets, with minimal background cytolysis in the control group (Figure 3E; N = 5, p < 0.0001). The median final stimulation was 3 (range 2–4; Figure S4), at which point all 2G CARs had greater tumor killing than did control T cells (Figure 3F; black asterisks, N = 5, p < 0.01). While no significant differences were observed between CD8α/CD28-, CD8α/41BB-, and CD28/CD28-CAR T cells, CD28/

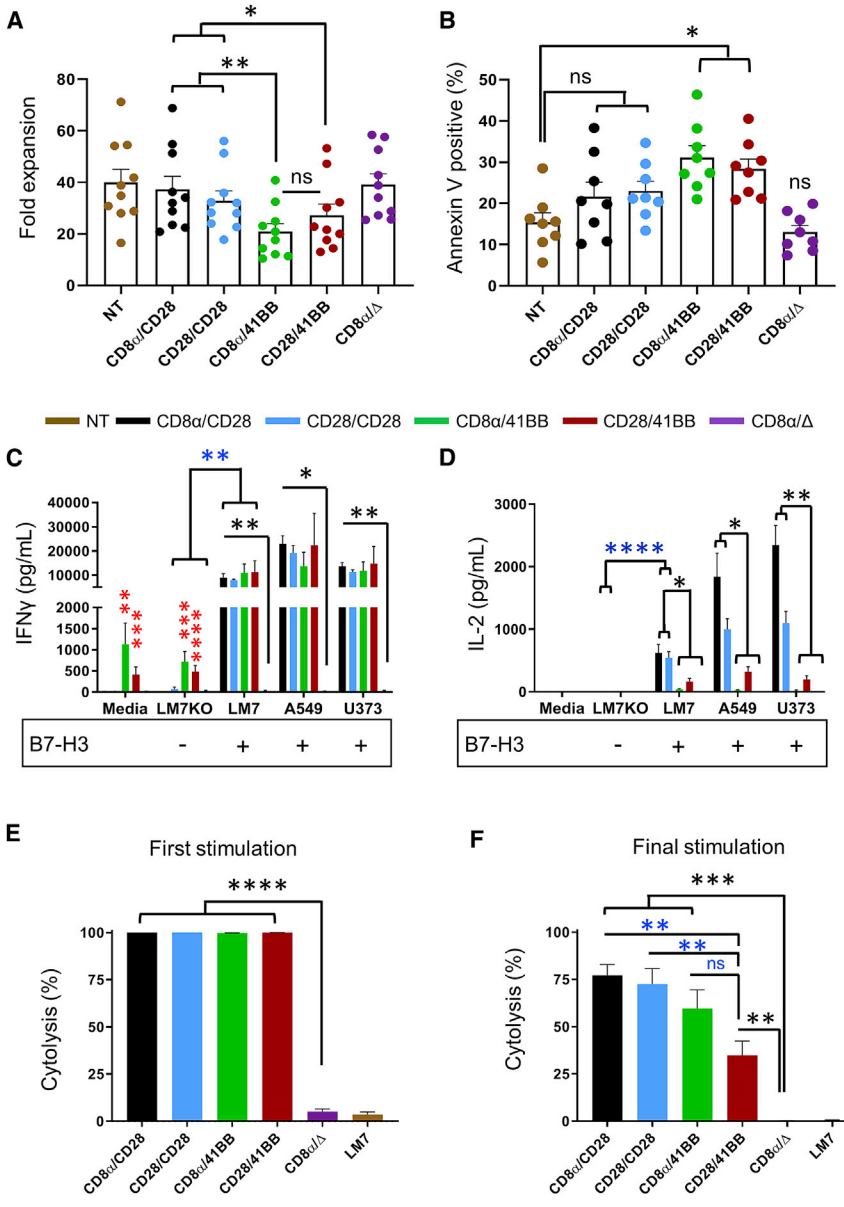

Figure 3. 2G B7-H3-CAR T Cell Expansion, Basal Apoptosis, Cytokine Secretion, and Repeat Killing Capacity

2G B7-H3-CAR T cells were evaluated for *in vitro* expansion and effector function. (A) Expansion of NT and CAR T cells (N = 10). (B) Basal apoptosis of NT and CAR T cells. (C and D) IFNγ (C) and IL-2 (D) production after coculture with B7-H3-positive (LM7, A549, U373) or B7-H3-negative (LM7KO) tumor cells, or media alone. Media were collected after 24 h and cytokines were determined by ELISA (N = 4 in duplicate; blue asterisks, LM7KO versus LM7 for functional CARs; black asterisks, CD8α/Δ versus functional CARs; red asterisks, CD8α/41BB-CAR or CD28/41BB-CAR versus CD8α/Δ-CAR in media alone or coculture with LM7KO). (E and F) Repeat impedance-based cytotoxicity assay (xCELLigence) using LM7 cells as targets and CAR T cells as effectors (N = 5 in triplicate). (E and F) First (E) and final (F) stimulation (black asterisks, CD8α/Δ-CAR versus functional CARs; blue asterisks or ns, CD28/41BB-CAR versus other functional CARs). One-way ANOVA was used for all analyses except for blue asterisks in (C) and (D) (two-way ANOVA). Data, mean ± SEM. *p < 0.05, **p < 0.01, ***p < 0.001, ****p < 0.0001. ns, not significant.

41BB-CAR T cells had significantly lower killing than did CAR T cells with CD28 costim domains (Figure 3F; blue asterisks; p < 0.01).

Expression of 41BBL on the Surface of B7-H3-CAR T Cells Enhances Their Effector Function *In Vitro*

While our 2G CAR studies gave initial insight into the function of CD28 and 41BB-CAR T cells, they did not explore whether activating both CD28 and 41BB signaling pathways is beneficial in B7-H3-CAR T cells. This was addressed in the following experiments for the CD8α/CD28-CAR, since it was consistently expressed at higher levels on the cell surface than the CD28/CD28-CAR. We compared two different forms of 41BB costimulation, which have been explored in other experimental systems.[21–25] We either inserted the 41BB signaling domain into the CD8α/CD28-CAR (CD8α/CD28.41BB), creating a 3G CAR, or generated a bicistronic LV encoding 41BBL, a 2A sequence, and the CD8α/CD28-CAR (41BBL) (Figure 4A; Figure S5).

Both LVs successfully transduced human T cells, as judged by VCN and percent surface expression, and expanded to similar levels (Figure 4B; Figures S6A–S6D). Phenotypic analysis demonstrated similar CD4- and CD8-positive T cell ratios; however, transduction with the 3G-CAR resulted in higher levels of central memory T cells (Figures S6E and S6F). To evaluate specificity and cytokine secretion, T cells were incubated with B7-H3-positive or B7-H3-negative tumors for 24 h. CD8α/CD28-, 3G-, or 41BBL-CAR T cells specifically recognized B7-H3-positive targets as judged by significant IFNγ production versus B7-H3-positive (LM7) compared to B7-H3-negative (LM7KO) tumor cells (Figure 4C; blue asterisks, N = 4, p < 0.01). In addition, CAR T cells recognized other B7-H3-positive tumor cells, including A549 and U373 (Figure 4C; black asterisks, N = 4, p < 0.05 for all constructs compared to control T cells). CD8α/CD28-, 3G-, or 41BBL-CAR T cells also produced significantly greater IL-2 in culture with LM7 compared to LM7KO (Figure 4D; blue asterisks, N = 4, p < 0.01) and compared to control T cells against all B7-H3-positive targets (Figure 4D; black asterisks, N = 4, p < 0.01, except comparing 3G CAR to CD8α/Δ against A549 = not significant [ns]).

To characterize cytolytic activity, CD8α/CD28-, 3G-, or 41BBL-CAR or control T cells were cocultured using the repeat killing assay

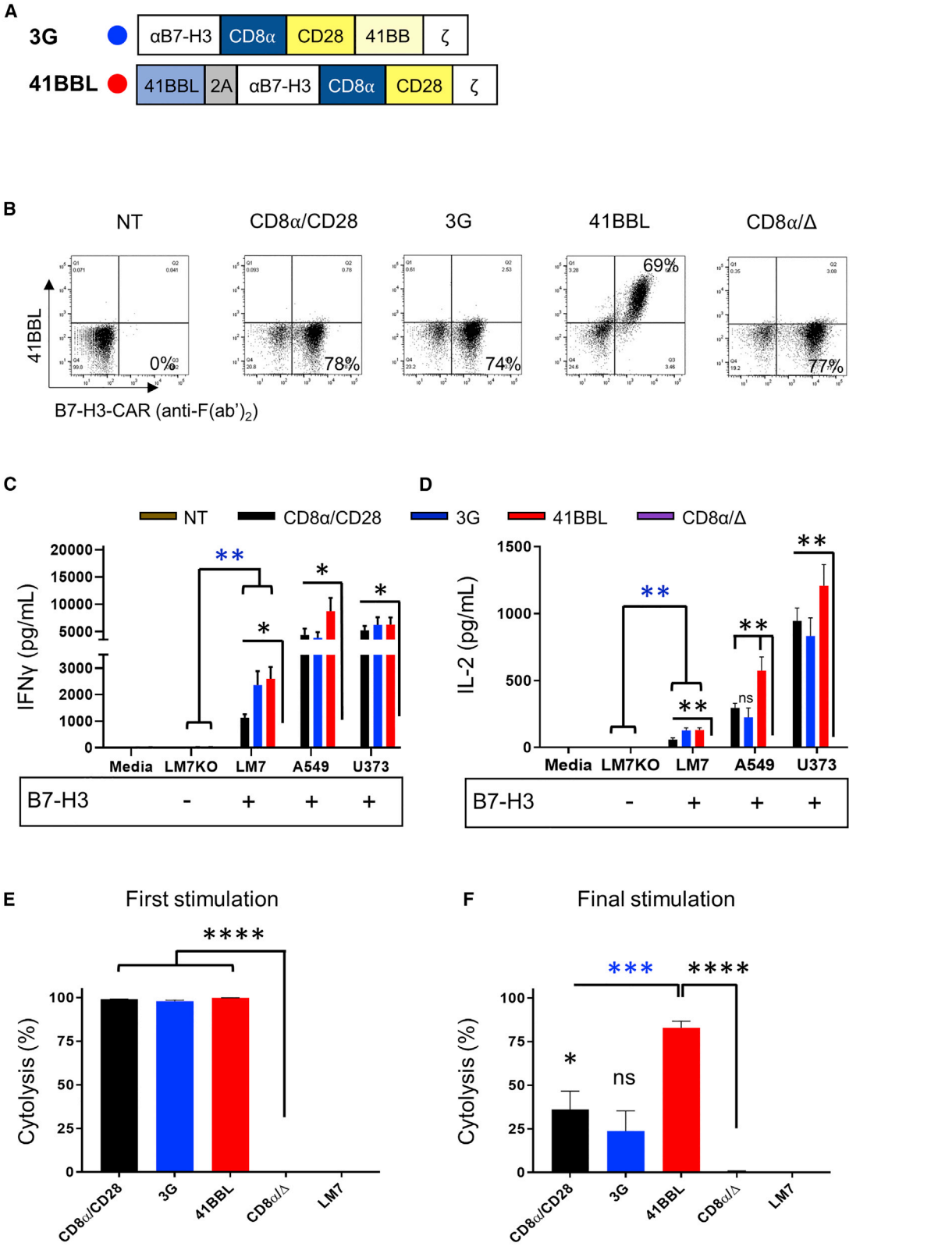

(legend on next page)

described above. All three B7-H3-CAR T cell types killed ~100% of targets after the first stimulation, with minimal cytolysis in the control group (Figure 4E; N = 4, p < 0.0001; Figure S7 shows individual stimulations for each donor). The median final stimulation was 3 (range 2–5; Figure S7). At final stimulation 41BBL-CAR T cells had significantly greater killing compared to CD8α/CD28- or 3G-CAR T cells (Figure 4F; blue asterisks, N = 4, p < 0.001) and compared to control T cells (Figure 4F; black asterisks, N = 4, p < 0.0001). Thus, expression of 41BBL on CD8α/CD28-CAR T cells significantly enhances their ability to repeatedly kill tumor cells.

CD8α/CD28- and 41BBL-CAR T Cells Have Enhanced Antitumor Activity *In Vivo*

Having shown that 41BBL-CAR T cells have improved antitumor activity after repeat exposure to B7-H3-positive tumor cells, we next compared the antitumor activity of 2G-CAR, 3G-CAR, 41BBL-CAR, or control T cells in three preclinical models as follows: (1) locoregional LM7 (Figures 5A and 5B), (2) systemic A549 (Figures 5C and 5D), and (3) systemic LM7 (Figures 5E and 5F). Given that CD28/41BB-CAR T cells had the lowest repeat killing capacity *in vitro*, we did not use this 2G product for *in vivo* testing. In all three models EGFP.firefly luciferase (ffLuc)-expressing tumor cells were used to allow for noninvasive tracking of tumor cell growth *in vivo*. In addition, low doses of CAR T cells were used to decipher differences between the antitumor activity of CAR T cell populations (locoregional LM7 model, 1×10^5 T cells; systemic A549 model, 3×10^6 T cells; systemic LM7 model, 1×10^6 T cells). In the locoregional LM7 and systemic A549 models, CD8α/CD28- and 41BBL-CAR T cells had superior antitumor activity in comparison to other CAR T cell populations, resulting in a significant survival advantage, with no significant differences between both constructs (Figures 5B and 5D; N = 5 mice/group, p < 0.01). In the systemic LM7 model, 41BBL-CAR T cells had improved antitumor activity in comparison to all other CAR T cell populations (Figure 5F; N = 5 mice/group, p < 0.01). In all three models, infusion of CD8α/41BB-CAR T cells did not improve survival in comparison to controls at the evaluated cell doses. Additionally, 3G-CAR T cells had limited antitumor activity. Furthermore, potent antitumor activity of CD8α/CD28- and 41BBL-CAR T cells was confirmed in the orthotopic U373 high-grade glioma (HGG) model (Figure S8).

To evaluate whether differences in antitumor activity between CAR T cell populations could be explained by differences in *in vivo* CAR T cell expansion, we injected EGFP.ffLuc-expressing CAR T cells into A549-bearing mice. 41BBL-CAR T cells persisted at significantly higher levels (N = 5, p < 0.01) starting on day 14 post-infusion in comparison to other CAR T cell populations (Figure 6A). 3G-CAR T cell persistence was the poorest, whereas CD8α/CD28- and CD8α/41BB-CAR T cell persistence was in-between. Since mice treated with CD8α/CD28- or 41BBL-CAR T cells survived long-term tumor-free in the locoregional LM7 model, we re-challenged four mice from each group with a second intraperitoneal (i.p.) dose of 1×10^6 LM7 tumor cells 133 days after initial tumor injection. Five mice without prior tumor or T cell injection received the same i.p. dose of LM7 cells as controls (tumor only). While tumors grew rapidly and resulted in death of control mice, those previously treated with CD8α/CD28- or 41BBL-CAR T cells had minimal tumor growth (Figure 6B) and survived to the end of the experiment (day 50 after tumor re-challenge; Figure 6C).

Collectively, the *in vivo* studies demonstrated that infused CD8α/CD28- and 41BBL-CAR T cells have potent antitumor activity and persist long-term in mice.

DISCUSSION

In this study, we describe the development and characterization of CARs that recognize the pediatric solid tumor antigen B7-H3. We show that 2G-CARs with a CD28 costim domain have superior antitumor activity in comparison to those with 41BB costimulation. In addition, we demonstrate that while incorporating a 41BB costim domain into the CD28-CAR is detrimental to effector function, expressing 41BBL on the surface of CD28-CAR T cells is beneficial.

Several studies have demonstrated that B7-H3 is expressed on a broad range of pediatric solid tumors and brain tumors.[7,10,26] However, most B7-H3 IHC protocols have not taken advantage of gene-editing technologies to validate B7-H3 immunoreactivity. In this study, we used such an approach to validate our staining protocol before evaluating pediatric solid tumors and normal tissues. We confirmed high B7-H3 expression in OS, rhabdomyosarcoma, DSRCT, and NBL as reported by others,[7,10,26] and in MPNST. However, B7-H3 expression in EWS was low to absent, which is in contrast to reports by other groups.[7,10] These discrepant results might be due to a small sample size since we and others have only stained a limited number of EWS tumors (less than 30 each), or due to different antibodies used to detect B7-H3 in each study.[7,10] We are planning to stain a larger set of EWS tumors in the future. Although so far not investigated for pediatric solid tumors, B7-H3 expression has been demonstrated in putative CD133-posititve cancer stem cell populations in colorectal cancer.[27]

Figure 4. Comparison of 2G-, 3G-, and 41BBL-CAR T Cell Effector Function *In Vitro*

(A) Schematic representation of the B7-H3-CAR with a CD8α/CD28 backbone combined with a 41BB endodomain (3G) or surface 41BB ligand (41BBL). (B) Representative flow plots of NT and transduced T cells. (C and D) IFNγ (C) and IL-2 (D) production after coculture with B7-H3-positive (LM7, A549, U373) or B7-H3-negative (LM7KO) tumor cells, or media alone. Media were collected after 24 h and cytokines were determined by ELISA (N = 4 in duplicate; blue asterisks, LM7KO versus LM7 for functional CARs; black asterisks and ns, CD8α/Δ-CAR versus functional CARs). (E and F) Repeat impedance-based cytotoxicity assay (xCELLigence) using LM7 cells as targets and CAR T cells as effectors (N = 4 in triplicate). First (E) and final (F) stimulation (black asterisks and ns, CD8α/Δ-CAR versus functional CARs; blue asterisks, 41BBL-CAR versus other functional CARs). One-way ANOVA was used for all analyses except for blue asterisks in (C) and (D) (two-way ANOVA). Data, mean ± SEM. *p < 0.05, **p < 0.01, ***p < 0.001, ****p < 0.0001. ns, non-significant.

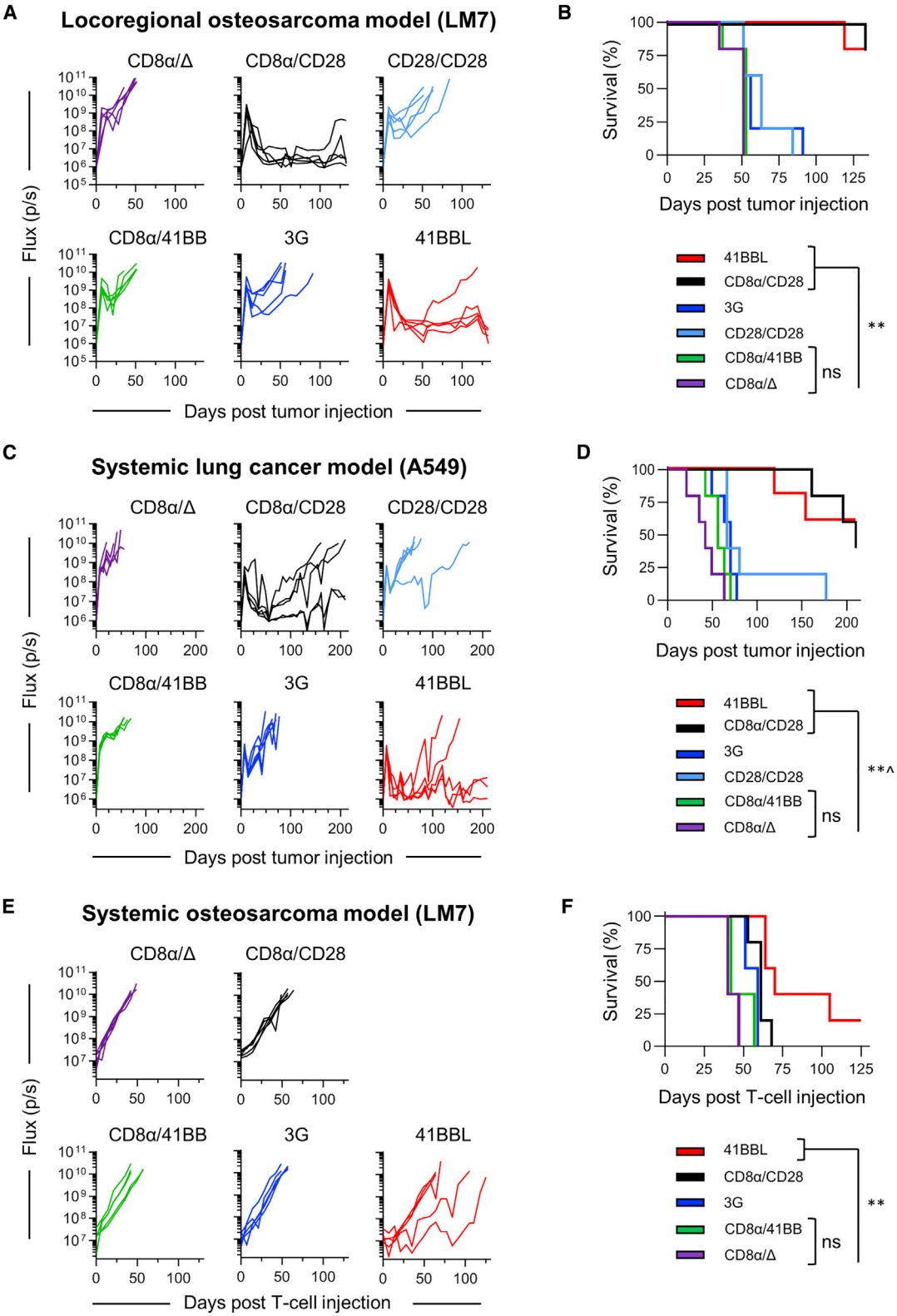

(legend on next page)

We also stained normal tissues and confirmed limited B7-H3 expression in normal tissues.[7,9,13] However, we found a high level of B7-H3 expression in non-neoplastic adrenal glands. High-level B7-H3 staining of adrenal glands has not been reported by other investigators,[7,13] and our findings need to be confirmed in an independent analysis. In addition, preclinical studies in immune-competent mouse models did not reveal adrenal toxicity of murine B7-H3-CAR T cells.[13] While the clinical experience with B7-H3 mAbs is limited, only 1 of 133 patients treated with PD-1 inhibitor plus B7-H3 mAb combination therapy experienced adrenal insufficiency,[28] a side effect previously reported with PD-1 inhibitor therapy alone.[29] In total, clinical monitoring for adrenal insufficiency, especially for early-phase clinical testing of B7-H3-CAR T cells, is advisable.

Despite intense research efforts and major advances in CAR technology, CAR design remains largely empirical.[30] We therefore designed a panel of LVs encoding different B7-H3-CARs and, with an MOI of 50, achieved a median VCN of 2.4 (±1.3) in CAR T cells, which is less than the upper VCN limit (<5.0) currently approved by the US Food and Drug Administration (FDA). We initially evaluated the outcome of combining different H/TM (CD8α or CD28) and costim (CD28 or 41BB) domains on the effector function of B7-H3-CAR T cells. 41BB-CAR T cells had impaired expansion, a high basal apoptosis rate, and secreted IFNγ in the absence of antigenic stimulation, indicating baseline or tonic signaling, which has been associated with decreased effector function.[31] Indeed, both 41BB-CAR T cell populations produced less IL-2 than did CD28-CAR T cells in the presence of B7-H3-positive tumor cells, and infusion of CD8α/41BB-CAR T cells did not improve survival of tumor-bearing mice compared to controls in three separate models. Our findings contrast with two recent studies that demonstrated potent antitumor activity of CD8α/41BB-CAR T cells in mice bearing B7-H3-positive tumors.[10,13] The observed differences are most likely due to several factors. First, we used a lower cell dose (1×10^5–3×10^6 CAR T cells/mouse) compared to the other studies, which used a cell dose of 1×10^7 CAR T cells/mouse for most of their experiments.[10,13] Second, one group used a different B7-H3-specific scFv (376.96) as an antigen recognition domain,[13] and several reports highlight that antigen recognition domains of CARs targeting the same antigen influence CAR function.[32,33] Lastly, transduction methods differed between our study and others (lentiviral versus gammaretroviral vectors), and at least one study highlighted that CAR T cells transduced with lentiviral or gammaretroviral vectors encoding the same CAR construct differ in their effector function.[34]

To investigate whether provision of 41BB costimulation enhances the effector function of our selected CD28-CAR, we compared two approaches. The first approach relied on incorporating the 41BB signaling domain in the 2G CD28-CAR, creating a 3G CAR, or expressing 41BBL on CD28-CAR T cells. While the former approach has been explored for numerous CARs, the latter approach has, so far, only been explored for 2G CD19-CARs, or prostate-specific membrane antigen (PSMA)-specific CARs lacking a CD28 costim domain.[21–23,35] In preclinical models the benefit of incorporating 41BB costimulation into 2G CARs has been model-dependent.[24,36,37] Direct comparison of 2G- and 3G-CAR T cells in humans is limited. However, one recent study compared the *in vivo* fate of 2G (CD28.ζ) and 3G (CD28.41BB.ζ) CD19-CAR T cells simultaneously infused into individual patients with CD19-positive non-Hodgkin's lymphoma.[38] 3G CD19-CAR T cells had greater expansion and persistence compared to 2G CD19-CAR T cells after lymphodepleting chemotherapy; however, it is unclear whether this enhanced anti-lymphoma activity. While there were no differences between the LVs encoding our 2G and 3G B7-H3-CARs, as judged by VCN and CAR expression, incorporating 41BB into the 2G CAR had deleterious effects on the ability of CAR T cells to kill tumors in our recursive killing assay and *in vivo*. Of note, incorporating 41BB into the CAR did not induce baseline IFNγ secretion, excluding tonic signaling of our 3G CAR as a potential explanation. Having both signaling molecules present might result in overactivation of 3G CAR T cells after activation, leading to activation-induced cell death. Alternatively, the configuration of the costim domains in the 3G CAR may alter CD28 and/or 41BB signaling, resulting in impaired effector function. Mechanistic studies to differentiate between both possibilities are in progress.

The second strategy we pursued to enhance the effector function of CD28-CAR T cells was to express 41BBL on their cell surface. This approach takes advantage of the activation-dependent expression of 41BB on the surface of conventional and CAR T cells.[39–41] Thus, there is a temporospatial separation of CD28 and 41BB costimulation in this approach, in contrast to a 3G CAR, in which both signals are provided simultaneously.[23] This approach has been studied in great detail for CD19-CAR T cells, and CD28-CAR T cells expressing 41BBL on their cell surface had superior effector function in comparison to 3G CD19-CAR T cells, and mechanistic studies revealed that activation of the IRF7/IFNβ pathway was critical.[23] While immune dysregulation has been observed in mice that transgenically express 41BBL, or in mice that received agonistic mAbs after hematopoietic cell transplantation,[42,43] CD28-CAR T cells expressing surface 41BBL were evaluated in a clinical trial for adults with CD19-positive malignancies (ClinicalTrials.gov: NCT03085173). Preliminary results of this clinical trial demonstrate that administration of these cells is

Figure 5. CD8α/CD28- and 41BBL-CAR T Cells Have Superior Antitumor Activity *In Vivo*

(A and B) Mice were injected with 1×10^6 LM7.ffLuc (OS) cells i.p. on day 0, followed by 1×10^5 CAR or control (CD8α/Δ) T cells i.p. on day 7. Bioluminescent signal (flux = photons/s) over time (A) and Kaplan-Meier survival curve (B) are shown. (C and D) NSG mice were injected i.v. with 2×10^6 A549.ffLuc (lung cancer) on day 0, followed by 3×10^6 CAR or control T cells on day 7. Bioluminescent signal over time (C) and Kaplan-Meier survival curve (D) are shown. (E and F) Mice were injected with 2×10^6 LM7.ffLuc cells i.v. on day −28, followed by injection of 1×10^6 CAR or control T cells i.v. 28 days later (day 0). Bioluminescent signal over time (E) and Kaplan-Meier survival curve for injected mice (F) are shown. The log-rank (Mantel-Cox) test was used to determine statistical significance between survival curves for all experiments. N = 5 mice per group. ^p = 0.0214 for 41BBL versus CD28/CD28, **p < 0.01. ns, not significant.

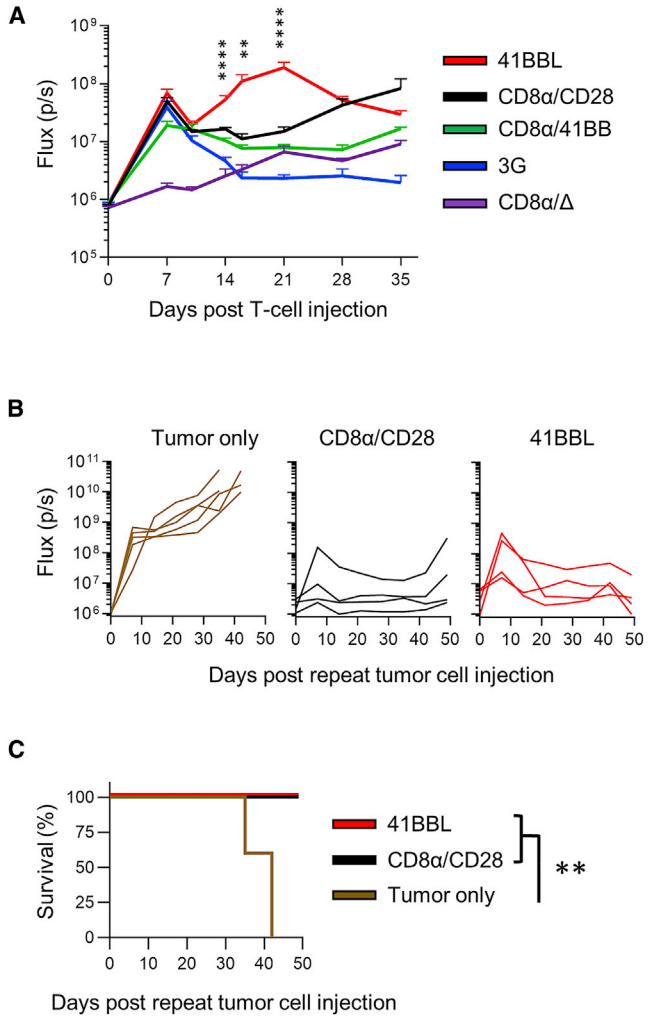

Figure 6. CAR T Cell Persistence and Repeat Tumor Challenge *In Vivo*

(A) NSG mice were injected with 2 × 10^6 A549 cells i.v. on day −7, followed by 1 × 10^6 ffLuc-expressing CAR or control (CD8α/Δ) T cells i.v. 7 days later (day 0). The graph depicts the T cell bioluminescent signal (flux = photons/s) over time (N = 5 per group; one-way ANOVA at indicated time points; mean ± SEM). (B and C) Mice treated with CD8α/CD28- or 41BBL-CAR T cells survived long-term tumor-free in the locoregional LM7 model and were re-challenged (N = 4 per group) with a second i.p. dose of 1 × 10^6 LM7.ffLuc tumor cells 133 days after the initial tumor injection. Five mice without prior tumor or T cell injection received the same i.p. dose of LM7 cells as controls (tumor only). (B) Bioluminescent signal over time. (C) Kaplan-Meier survival curve after repeat tumor challenge. Survival data were analyzed using the log-rank (Mantel-Cox) test. **p < 0.01, ****p < 0.0001.

safe and efficacacious.[35] In the present study, we explored whether cell surface expression of 41BBL enhances the effector function of B7-H3-CAR T cells. Our results demonstrate that provision of 41BB costimulation through this route enhances the capability of CD28-CAR T cells to sequentially kill tumor cells, expand *in vivo*, and have greater antitumor activity in one of four tumor models evaluated. These results are consistent with studies by others indicating that the benefit of 41BB costimulation in the context of CD28-CAR is model-dependent.[24,37] Of note, 41BBL CAR T cells had a lower percentage of central memory T cells compared to 3G CAR T cells. While pre-clinical and clinical evidence suggests that a lower percentage of naive or central memory T cells is associated with decreased *in vivo* expansion of CD19-CAR T cells,[44] the benefit of memory phenotype for other CAR T cell products, especially those targeting solid tumors, is largely unknown. Based on our pre-clinical data, the memory phenotype does not appear to affect efficacy in our model.

In summary, using an scFv derived from mAb MGA271, CD28-CAR T cells have superior antitumor activity than 41BB-CAR T cells for targeting B7-H3-positive tumors. In addition, we demonstrate that their effector function can be further enhanced by expressing 41BBL on the cell surface and not by incorporating 41BB into the endodomain. While we have selected 41BBL-CAR T cells for future clinical testing, our study also serves as a reminder that CAR design remains largely empirical, necessitating careful analysis of multiple constructs *in vitro* as well as in a panel of animal models.

MATERIALS AND METHODS

Human Solid Tumor and Normal Tissue Samples

Archived pediatric solid tumor samples were obtained from multiple surgical sources (resection, autopsy) and constructed into TMAs. Each solid tumor TMA was constructed in duplicate and consisted of a grid of 2-mm cores. Adult normal tissue samples were provided by the Cooperative Human Tissue Network (CHTN), which is funded by the National Cancer Institute. Other investigators may have received specimens from the same CHTN tissue specimens. Additional pediatric whole-section non-neoplastic adrenal glands were obtained from autopsies (n = 5) or surgical resections that included removal of adrenal tissue (n = 5). The St. Jude Children's Research Hospital Institutional Review Board deemed that these studies do not constitute human subjects research.

IHC

Formalin-fixed, paraffin-embedded sections were cut at 4 μm, collected onto charged slides, stained on a Leica BOND-III Immunostainer (Leica Biosystems, Germany) after 20 min of heat-induced epitope retrieval (ER2, EDTA [pH 9], Leica Biosystems), and incubated with a 1:50 dilution of monoclonal rabbit B7-H3 antibody (clone D9ML, Cell Signaling Technology, Danvers, MA, USA) for 30 min at room temperature, followed by visualization of a chromogenic signal with the Refine Polymer diaminobenzidine (DAB) detection kit (Leica Biosystems). The antibody protocol was developed on solid tumor-derived xenografts from LM7 wild-type (B7-$H3^{+/+}$) and LM7 B7-H3-KO (B7-$H3^{-/-}$) cells grown in non-obese diabetic (NOD)-*scid* IL2Rγ^{null} (NSG) mice. The intensity of B7-H3 staining was scored as 0 for no positivity, 1 for weak positivity, 2 for moderate positivity, and 3 for strong positivity. Total B7-H3 positivity was enumerated using an H-score (range 0–300) determined by summing the product of the intensity score by the percentage of cells stained positive at each intensity.

B7-H3 KO Cells

B7-H3$^{-/-}$ LM7 cells (LM7KO) were generated using CRISPR-Cas9 technology. Briefly, 400,000 LM7 cells were transiently transfected with precomplexed ribonucleoproteins (RNPs) consisting of 150 pmol of chemically modified single guide RNA (sgRNA) (5′-GAUCAAACA GAGCUGUGAGG-3′, Synthego) and 35pmol of Cas9 protein (St. Jude Protein Production Core) via nucleofection (4D-Nucleofector X unit; Lonza, Switzerland) using solution P3 and program DS-150 in a small (20-μL) cuvette according to the manufacturer's recommended protocol. A portion of the pool of cells was harvested 3 days after nucleofection and verified to contain the desired modification via targeted deep sequencing and analysis with CRIS.py.[45] Post-nucleofection LM7KO cells were stained with B7-H3 antibody (clone 7-517; Becton Dickinson, Franklin Lakes, NJ, USA) and sorted on the B7-H3-negative population using a BD FACSAria III instrument. This sorting step was repeated one additional time to produce a final LM7KO product. After KO and flow sorting, LM7KO cells were authenticated by short tandem repeat (STR) profiling using the service of the American Type Culture Collection (FTA sample collection kit; ATCC, Manassas, VA, USA).

Cell Lines

The metastatic OS cell line, LM7, was kindly provided by Dr. Eugenie Kleinerman (MD Anderson Cancer Center, Houston, TX, USA). The A549 (lung cancer), U373 (HGG), and KG1A (acute myeloid leukemia [AML]) cell lines were purchased from ATCC. LM7, A549, and U373 cells expressing EGFP and ffLuc were previously described.[46–48] All adherent cell lines were grown in DMEM (GE Healthcare, Marlborough, MA, USA), supplemented with 10% fetal bovine serum (FBS) (GE Healthcare) and 1% GlutaMAX (Thermo Fisher Scientific, Waltham, MA, USA), and sub-cultured with 0.05% trypsin-EDTA (Thermo Fisher Scientific). KG1A cells were grown in Iscove's modified Dulbecco's medium (IMDM) (Thermo Fisher Scientific) supplemented with 20% FBS and 1% GlutaMAX. All cells were maintained at 37°C in 5% CO_2. Cell lines were authenticated by STR profiling as described above, and routinely checked for mycoplasma using the MycoAlert mycoplasma detection kit (Lonza).

Generation of B7-H3-CAR LVs

The LV backbone used for this study has been previously described,[49] except the insulators were removed from the self-inactivating 3′ partially deleted viral LTRs based on the safety records of LVs in clinical trials.[50] The expression cassette of the LV is under control of the MND promoter (myeloproliferative sarcoma virus enhancer, negative control region deleted, dl587rev primer-binding site substituted). Minigenes encoding B7-H3-CARs (Figures 2A and 4A), derived from the mAb MGA271, were synthesized by GeneArt (Thermo Fisher Scientific) and subcloned by standard techniques. All cloned B7-H3-CAR constructs were verified by sequencing (Hartwell Center, St. Jude Children's Research Hospital, Memphis, TN, USA). LVs were produced as previously described.[51] Briefly, 293T cells (ATCC CLR-11268), adapted to grow in suspension using serum-free media, were transfected with the transfer vector and helper plasmids, pCAG-kGP1-1R-AF, pCAG-vesicular stomatitis virus glycoprotein G (VSVG))-AF, and pCMV-Rev-AF expressing HIV-1 *gagpol*, the vesicular stomatitis virus glycoprotein, and HIV-1 Rev, respectively. Forty-eight hours later, the supernatant was harvested by a combination of centrifugation and 0.22 μm filtration to remove cell debris. LV particles were purified by high-performance liquid chromatography (HPLC) and titered on HOS cells as previously described.[51]

Generation of B7-H3-CAR T Cells

Human peripheral blood mononuclear cells (PBMCs) were obtained from whole blood of healthy donors under an Institutional Review Board (IRB)-approved protocol at St. Jude Children's Research Hospital, after informed consent was obtained in accordance with the Declaration of Helsinki. To generate CAR T cells, PBMCs were isolated by Lymphoprep (Abbott Laboratories, Abbott Park, IL, USA) gradient centrifugation. On day 0, $CD4^+$ and $CD8^+$ T cells were enriched from PBMCs by immunomagnetic separation using CD4 and CD8 microbeads (Miltenyi, Germany), an LS column (Miltenyi), and a MidiMACS separator (Miltenyi). Enriched T cells were resuspended at 1×10^6 cells/mL in RPMI 1640 (GE Healthcare) supplemented with 10% FBS (GE Healthcare), 1% GlutaMAX (Thermo Fisher Scientific), and cytokines IL-7 and IL-15 (10 ng/mL each) (Biological Resources Branch, National Cancer Institute, Frederick, MD, USA, and PeproTech, Rocky Hill, NJ, USA) and stimulated overnight on 24-well non-tissue culture-treated plates that were precoated with CD3 and CD28 antibodies (Miltenyi). Transduction was performed on day 1 by adding VSVG-pseudotyped LV particles at an MOI of 50, and protamine sulfate at 4 μg/mL. On day 4, T cells were transferred into new 24-well tissue culture-treated plates and subsequently expanded with IL-7 and IL-15 (10 ng/mL each). All experiments were performed 7–14 days post-transduction. Biological replicates were performed using PBMCs from different healthy donors.

VCN

Transduced T cells were harvested and total genomic DNA was isolated using the Zymo Research Quick-DNA 96 kit (Zymo Research, Irvine, CA, USA). To determine the VCN per cell, genomic DNA was digested with MspI and used as a template in PCR using a digital droplet PCR (ddPCR) instrument (QX200; Bio-Rad, Hercules, CA, USA). The following primer-probe sets were used to amplify the HIV psi sequence located on the vector genome and the endogenous control gene RPP30, 5′-ACTTGAAAGCGAAAGGGAAAC-3′, 5′-CACCCATCTCTCTCCTTCTAGCC-3′, and probe 5′-FAM-AGC TCTCTCGACGCAGGACTCGGC-3′ and 5′-GCGGCTGTCTCCA CAAGT-3′, 5′-GATTTGGACCTGCGAGCG-3′ and probe 5′-HEX-CTGACCTGAAGGCTCT-3′, respectively. The reaction mixture contained ddPCR Supermix for probes without uridine 5′-triphosphate (UTP) (Bio-Rad). The cycled droplets were read with the QX200 droplet reader (Bio-Rad). The ratio of the numbers of molecules of these two genes is the sample's gene of interest relative copy number analyzed with QuantaSoft droplet reader software version 1.7.4.0917 (Bio-Rad).

Flow Cytometry

A FACSCanto II (BD Biosciences) instrument was used to acquire flow cytometry data, which was analyzed using FlowJo v10 (BD

Biosciences). For surface staining, samples were washed with and stained in PBS (Lonza) with 1% FBS (GE Healthcare). For all experiments, matched isotypes or known negatives (e.g., NT T cells) served as gating controls. CAR detection was performed using $F(ab')_2$ fragment=specific antibody (polyclonal, Jackson ImmunoResearch, West Grove, PA, USA). T cells were stained with fluorochrome-conjugated antibodies using combinations of the following markers: CD4 (clone SK3, BD Biosciences), CD8 (clone SK1, BD Biosciences), CCR7 (clone G043H7, BioLegend, San Diego, CA, USA), CD45RO (clone UCHL1, BD Biosciences), and 41BBL (clone 5F4, BioLegend). Tumor cell lines were evaluated for expression of B7-H3 using B7-H3 antibody (clone 7-517, BD Biosciences, or clone FM276, Miltenyi). To determine apoptosis, T cells were labeled with annexin V (BD Biosciences) and DAPI (BD Biosciences). The percentages of apoptotic cells were determined by the percent annexin V positive.

Analysis of Cytokine Production

5×10^5 T cells were cocultured with no tumor cells or 5×10^5 LM7KO, LM7, A549, or U373 cells, without the provision of exogenous cytokines. Approximately 24 h after coculture, supernatant was collected and frozen for later analysis. Production of IFNγ and IL-2 was measured using a quantitative ELISA per the manufacturer's instructions (R&D Systems, Minneapolis, MN, USA).

Cytotoxicity and Repeat Killing Assays

The xCELLigence real-time cell analyzer (RTCA) MP instrument (Agilent Technologies, Santa Clara, CA, USA) was used to assess CAR T cell cytotoxicity and repeat killing capacity. All assays were performed in triplicate and without the addition of exogenous cytokines. First, 30,000 LM7 cells in complete RPMI were added to each well of a 96-well E-Plate (Agilent). After LM7 cells adhered to the E-Plate for approximately 24 h and reached a cell index (relative cell impedance) plateau, 15,000 T cells in complete RPMI were added. LM7 cells alone served as negative controls. The cell index was monitored every 15 min for 3 days and normalized to the maximum cell index value immediately prior to T cell plating. Percent cytotoxicity was calculated using the RTCA Software Pro immunotherapy module (Agilent).[52] For repeat killing assays, 72 h after T cell plating, media and T cells were gently removed to avoid disrupting adherent LM7 cells and plated on 30,000 fresh LM7 cells adhered to a new 96-well E-Plate. Repeat cytolysis was assessed until T cells stopped killing, defined by no CAR T cell killing greater than 50% of LM7 target cells, or over a maximum of five total stimulations per donor.

Xenograft Mouse Models

Animal experiments followed a protocol approved by the St. Jude Children's Research Hospital Institutional Animal Care and Use Committee. All experiments utilized 8- to 12-week-old male or female NSG mice purchased from The Jackson Laboratory (Bar Harbor, ME, USA) or obtained from the St. Jude NSG colony. Mice were euthanized when they reached our bioluminescent flux endpoint of 1×10^{10} photons/s, or when they met physical euthanasia criteria (significant weight loss, signs of distress), or when recommended by the St. Jude veterinary staff. For the local OS model, mice received an i.p. injection of 1×10^6 LM7.eGFP.ffLuc cells and, 7 days later, an i.p. injection of 1×10^5 CAR T cells. For the systemic lung cancer model, 2×10^6 A549.eGFP.ffLuc cells were injected intravenously (i.v.). Seven days later 3×10^6 CAR T cells were injected i.v. For the systemic OS model, 2×10^6 LM7.eGFP.ffLuc cells were injected i.v. Twenty-eight days later 1×10^6 CAR T cells were injected i.v. For the orthotopic HGG model, NSG mice were injected with 5×10^4 U373.eGFP.ffLuc cells intracranially (i.c.). Seven days later 2×10^6 CAR T cells were injected i.c. For the CAR T cell expansion model, 2×10^6 A549 cells were injected i.v., followed by 1×10^6 ffLuc labeled T cells 7 days later. For the repeat tumor challenge locoregional OS model, mice that were initially treated with CD8α/CD28- or 41BBL-CAR T cells received a second dose of 1×10^6 LM7.eGFP.ffLuc tumor cells 133 days after the initial tumor cell injection. Five mice that received no previous tumor or CAR T cell infusion served as controls.

Bioluminescent Imaging

Mice were injected i.p. with 150 mg/kg of D-luciferin 5–10 minutes before imaging, anesthetized with isoflurane (1.5%–2% delivered in 100% O_2 at 1 L/min), and imaged with an *in vivo* imaging system (IVIS) 200 (PerkinElmer, Waltham, MA, USA). The photons emitted from the luciferase-expressing cells were quantified using Living Image software (PerkinElmer). Mice were imaged once per week to track tumor burden, and one to two times per week to track T cells.

Statistical Analysis

For comparison of three or more groups with a single independent variable, statistical significance was determined by one-way ANOVA with a Tukey's multiple comparison test. For comparison of three or more groups with two or more independent variables, statistical significance was determined by two-way ANOVA with Sidak's multiple comparison test. Survival curves were plotted using the Kaplan-Meier method. Statistical significance between survival curves was determined using the log-rank (Mantel-Cox) test.

SUPPLEMENTAL INFORMATION

Supplemental Information can be found online at https://doi.org/10.1016/j.omto.2020.06.018.

AUTHOR CONTRIBUTIONS

Conception and design: S.G. and C.D. Development of methodology: P.N., E.O., M.C., J.J., S.P.-M., J.P., J.M., S.Z., R.T., G.K., S.G., and C.D. Acquisition of data: P.N., E.O., M.C., D.H., J.J., C.O., J.M., and G.K. Analysis and interpretation of data: P.N., E.O., M.C., D.H., C.O., G.K., S.G., and C.D. Writing, review, and/or revision of manuscript: all authors. Study supervision: S.G. and C.D.

CONFLICTS OF INTEREST

The authors have patent and patent applications in the field of cell and gene therapy for cancer, including a patent application for B7-H3-specific CAR T cells. S.G. has a research collaboration with TESSA therapeutics and is a member of the data safety monitoring board of Immatics US.

ACKNOWLEDGMENTS

This work was supported by National Institutes of Health (NIH) grant K12CA0904335, The Assisi Foundation of Memphis, the Rally Foundation for Childhood Cancer Research, The Truth 365, the Sarcoma Foundation of America, The Matthew Larson Foundation for Pediatric Brain Tumors, and by the American Lebanese Syrian Associated Charities. Animal imaging was performed by the St. Jude Center for In Vivo Imaging and Therapeutics, which is supported in part by NIH grants P01CA096832 and R50CA211481. Genome engineering/cell line creation was performed by the Center for Advanced Genome Engineering, which is supported in part by NCI/NIH grant P30CA021765. RNA sequencing was performed by the Hartwell Center, which is supported in part by the National Cancer Institute of the National Institutes of Health under award no. P30CA021765. The content is solely the responsibility of the authors and does not necessarily represent the official views of the National Institutes of Health. We thank Deanna Langfitt for her brilliance and providing advice and technical support for flow cytometry experiments. We thank the Cooperative Human Tissue Network, which is funded by the National Cancer Institute, for providing high-quality normal tissue samples. The graphical abstract was modified from a graphic created with BioRender.com. We thank Elizabeth R. Stevens, St. Jude Biomedical Communications Graphic Design, for expertise and contributions to enhance our graphical abstract.

REFERENCES

1. Ward, E., DeSantis, C., Robbins, A., Kohler, B., and Jemal, A. (2014). Childhood and adolescent cancer statistics, 2014. CA Cancer J. Clin. *64*, 83–103.
2. Spraker-Perlman, H.L., Barkauskas, D.A., Krailo, M.D., Meyers, P.A., Schwartz, C.L., Doski, J., Gorlick, R., Janeway, K.A., and Isakoff, M.S. (2019). Factors influencing survival after recurrence in osteosarcoma: a report from the Children's Oncology Group. Pediatr. Blood Cancer *66*, e27444.
3. Lagmay, J.P., Krailo, M.D., Dang, H., Kim, A., Hawkins, D.S., Beaty, O., 3rd, Widemann, B.C., Zwerdling, T., Bomgaars, L., Langevin, A.M., et al. (2016). Outcome of patients with recurrent osteosarcoma enrolled in seven phase II trials through Children's Cancer Group, Pediatric Oncology Group, and Children's Oncology Group: learning from the past to move forward. J. Clin. Oncol. *34*, 3031–3038.
4. Stahl, M., Ranft, A., Paulussen, M., Bölling, T., Vieth, V., Bielack, S., Görtitz, I., Braun-Munzinger, G., Hardes, J., Jürgens, H., and Dirksen, U. (2011). Risk of recurrence and survival after relapse in patients with Ewing sarcoma. Pediatr. Blood Cancer *57*, 549–553.
5. Pappo, A.S., Anderson, J.R., Crist, W.M., Wharam, M.D., Breitfeld, P.P., Hawkins, D., Raney, R.B., Womer, R.B., Parham, D.M., Qualman, S.J., and Grier, H.E. (1999). Survival after relapse in children and adolescents with rhabdomyosarcoma: a report from the Intergroup Rhabdomyosarcoma Study Group. J. Clin. Oncol. *17*, 3487–3493.
6. London, W.B., Castel, V., Monclair, T., Ambros, P.F., Pearson, A.D., Cohn, S.L., Berthold, F., Nakagawara, A., Ladenstein, R.L., Iehara, T., and Matthay, K.K. (2011). Clinical and biologic features predictive of survival after relapse of neuroblastoma: a report from the International Neuroblastoma Risk Group project. J. Clin. Oncol. *29*, 3286–3292.
7. Modak, S., Kramer, K., Gultekin, S.H., Guo, H.F., and Cheung, N.K. (2001). Monoclonal antibody 8H9 targets a novel cell surface antigen expressed by a wide spectrum of human solid tumors. Cancer Res. *61*, 4048–4054.
8. Loo, D., Alderson, R.F., Chen, F.Z., Huang, L., Zhang, W., Gorlatov, S., Burke, S., Ciccarone, V., Li, H., Yang, Y., et al. (2012). Development of an Fc-enhanced anti-B7-H3 monoclonal antibody with potent antitumor activity. Clin. Cancer Res. *18*, 3834–3845.
9. Seaman, S., Zhu, Z., Saha, S., Zhang, X.M., Yang, M.Y., Hilton, M.B., Morris, K., Szot, C., Morris, H., Swing, D.A., et al. (2017). Eradication of tumors through simultaneous ablation of CD276/B7-H3-positive tumor cells and tumor vasculature. Cancer Cell *31*, 501–515.e8.
10. Majzner, R.G., Theruvath, J.L., Nellan, A., Heitzeneder, S., Cui, Y., Mount, C.W., Rietberg, S.P., Linde, M.H., Xu, P., Rota, C., et al. (2019). CAR T cells targeting B7-H3, a pan-cancer antigen, demonstrate potent preclinical activity against pediatric solid tumors and brain tumors. Clin. Cancer Res. *25*, 2560–2574.
11. Hofmeyer, K.A., Ray, A., and Zang, X. (2008). The contrasting role of B7-H3. Proc. Natl. Acad. Sci. USA *105*, 10277–10278.
12. Leitner, J., Klauser, C., Pickl, W.F., Stöckl, J., Majdic, O., Bardet, A.F., Kreil, D.P., Dong, C., Yamazaki, T., Zlabinger, G., et al. (2009). B7-H3 is a potent inhibitor of human T-cell activation: no evidence for B7-H3 and TREML2 interaction. Eur. J. Immunol. *39*, 1754–1764.
13. Du, H., Hirabayashi, K., Ahn, S., Kren, N.P., Montgomery, S.A., Wang, X., Tiruthani, K., Mirlekar, B., Michaud, D., Greene, K., et al. (2019). Antitumor responses in the absence of toxicity in solid tumors by targeting B7-H3 via chimeric antigen receptor T cells. Cancer Cell *35*, 221–237.e8.
14. Nehama, D., Di Ianni, N., Musio, S., Du, H., Patané, M., Pollo, B., Finocchiaro, G., Park, J.J.H., Dunn, D.E., Edwards, D.S., et al. (2019). B7-H3-redirected chimeric antigen receptor T cells target glioblastoma and neurospheres. EBioMedicine *47*, 33–43.
15. Tang, X., Zhao, S., Zhang, Y., Wang, Y., Zhang, Z., Yang, M., Zhu, Y., Zhang, G., Guo, G., Tong, A., and Zhou, L. (2019). B7-H3 as a novel CAR-T therapeutic target for glioblastoma. Mol. Ther. Oncolytics *14*, 279–287.
16. Ahmed, N., Brawley, V.S., Hegde, M., Robertson, C., Ghazi, A., Gerken, C., Liu, E., Dakhova, O., Ashoori, A., Corder, A., et al. (2015). Human epidermal growth factor receptor 2 (HER2)-specific chimeric antigen receptor-modified T cells for the immunotherapy of HER2-positive sarcoma. J. Clin. Oncol. *33*, 1688–1696.
17. Beatty, G.L., O'Hara, M.H., Lacey, S.F., Torigian, D.A., Nazimuddin, F., Chen, F., Kulikovskaya, I.M., Soulen, M.C., McGarvey, M., Nelson, A.M., et al. (2018). Activity of mesothelin-specific chimeric antigen receptor T cells against pancreatic carcinoma metastases in a phase 1 trial. Gastroenterology *155*, 29–32.
18. Krenciute, G., Prinzing, B.L., Yi, Z., Wu, M.F., Liu, H., Dotti, G., Balyasnikova, I.V., and Gottschalk, S. (2017). Transgenic expression of IL15 improves antiglioma activity of IL13Rα2-CAR T cells but results in antigen loss variants. Cancer Immunol. Res. *5*, 571–581.
19. Sukumaran, S., Watanabe, N., Bajgain, P., Raja, K., Mohammed, S., Fisher, W.E., Brenner, M.K., Leen, A.M., and Vera, J.F. (2018). Enhancing the potency and specificity of engineered T cells for cancer treatment. Cancer Discov. *8*, 972–987.
20. Ren, J., Liu, X., Fang, C., Jiang, S., June, C.H., and Zhao, Y. (2017). Multiplex genome editing to generate universal CAR T cells resistant to PD1 inhibition. Clin. Cancer Res. *23*, 2255–2266.
21. Pulè, M.A., Straathof, K.C., Dotti, G., Heslop, H.E., Rooney, C.M., and Brenner, M.K. (2005). A chimeric T cell antigen receptor that augments cytokine release and supports clonal expansion of primary human T cells. Mol. Ther. *12*, 933–941.
22. Stephan, M.T., Ponomarev, V., Brentjens, R.J., Chang, A.H., Dobrenkov, K.V., Heller, G., and Sadelain, M. (2007). T cell-encoded CD80 and 4-1BBL induce auto- and transcostimulation, resulting in potent tumor rejection. Nat. Med. *13*, 1440–1449.
23. Zhao, Z., Condomines, M., van der Stegen, S.J.C., Perna, F., Kloss, C.C., Gunset, G., Plotkin, J., and Sadelain, M. (2015). Structural design of engineered costimulation determines tumor rejection kinetics and persistence of CAR T cells. Cancer Cell *28*, 415–428.
24. Carpenito, C., Milone, M.C., Hassan, R., Simonet, J.C., Lakhal, M., Suhoski, M.M., Varela-Rohena, A., Haines, K.M., Heitjan, D.F., Albelda, S.M., et al. (2009). Control of large, established tumor xenografts with genetically retargeted human T cells containing CD28 and CD137 domains. Proc. Natl. Acad. Sci. USA *106*, 3360–3365.
25. Santoro, S.P., Kim, S., Motz, G.T., Alatzoglou, D., Li, C., Irving, M., Powell, D.J., Jr., and Coukos, G. (2015). T cells bearing a chimeric antigen receptor against prostate-specific membrane antigen mediate vascular disruption and result in tumor regression. Cancer Immunol. Res. *3*, 68–84.

26. Wang, L., Zhang, Q., Chen, W., Shan, B., Ding, Y., Zhang, G., Cao, N., Liu, L., and Zhang, Y. (2013). B7-H3 is overexpressed in patients suffering osteosarcoma and associated with tumor aggressiveness and metastasis. PLoS ONE *8*, e70689.

27. Bin, Z., Guangbo, Z., Yan, G., Huan, Z., Desheng, L., and Xueguang, Z. (2014). Overexpression of B7-H3 in $CD133^+$ colorectal cancer cells is associated with cancer progression and survival in human patients. J. Surg. Res. *188*, 396–403.

28. Aggarwal, C., Joshua, A., Ferris, R., Antonia, S., Rahma, E.E., Tolcher, A., Cohen, R.B., Lou, Y., Ralph Hauke, R., Vogelzang, N., et al. (2018). A phase 1, open-label, dose-escalation study of enoblituzumab in combination with pembrolizumab in patients with select solid tumors. In: Meeting Abstracts of the 33rd Annual Meeting and Pre-Conference Programs of the Society for Immunotherapy of Cancer (SITC 2018), abstract O24, https://www.macrogenics.com/wp-content/uploads/2015/09/SITC-2018-O24-Enoblituzumab-Pembrolizumab-Ph-1-Data.pdf.

29. Tan, M.H., Iyengar, R., Mizokami-Stout, K., Yentz, S., MacEachern, M.P., Shen, L.Y., Redman, B., and Gianchandani, R. (2019). Spectrum of immune checkpoint inhibitors-induced endocrinopathies in cancer patients: a scoping review of case reports. Clin. Diabetes Endocrinol. *5*, 1.

30. Guedan, S., Calderon, H., Posey, A.D., Jr., and Maus, M.V. (2018). Engineering and design of chimeric antigen receptors. Mol. Ther. Methods Clin. Dev. *12*, 145–156.

31. Long, A.H., Haso, W.M., Shern, J.F., Wanhainen, K.M., Murgai, M., Ingaramo, M., Smith, J.P., Walker, A.J., Kohler, M.E., Venkateshwara, V.R., et al. (2015). 4-1BB costimulation ameliorates T cell exhaustion induced by tonic signaling of chimeric antigen receptors. Nat. Med. *21*, 581–590.

32. Haso, W., Lee, D.W., Shah, N.N., Stetler-Stevenson, M., Yuan, C.M., Pastan, I.H., Dimitrov, D.S., Morgan, R.A., FitzGerald, D.J., Barrett, D.M., et al. (2013). Anti-CD22-chimeric antigen receptors targeting B-cell precursor acute lymphoblastic leukemia. Blood *121*, 1165–1174.

33. Hudecek, M., Lupo-Stanghellini, M.T., Kosasih, P.L., Sommermeyer, D., Jensen, M.C., Rader, C., and Riddell, S.R. (2013). Receptor affinity and extracellular domain modifications affect tumor recognition by ROR1-specific chimeric antigen receptor T cells. Clin. Cancer Res. *19*, 3153–3164.

34. Gomes-Silva, D., Mukherjee, M., Srinivasan, M., Krenciute, G., Dakhova, O., Zheng, Y., Cabral, J.M.S., Rooney, C.M., Orange, J.S., Brenner, M.K., and Mamonkin, M. (2017). Tonic 4-1BB costimulation in chimeric antigen receptors impedes T cell survival and is vector-dependent. Cell Rep. *21*, 17–26.

35. Park, J.H., Palomba, M.L., Batlevi, C.L., Riviere, I., Wang, X., Senechal, B., Furman, R.R., Bernal, Y., Hall, M., Pineda, J., et al. (2018). A phase I first-in-human clinical trial of CD19-targeted 19-28z/4-1BBL "armored" CAR T cells in patients with relapsed or refractory NHL and CLL including Richter's transformation. Blood *132* (*Suppl. 1*), 224.

36. Zhong, X.S., Matsushita, M., Plotkin, J., Riviere, I., and Sadelain, M. (2010). Chimeric antigen receptors combining 4-1BB and CD28 signaling domains augment PI3kinase/AKT/Bcl-X_L activation and $CD8^+$ T cell-mediated tumor eradication. Mol. Ther. *18*, 413–420.

37. Abate-Daga, D., Lagisetty, K.H., Tran, E., Zheng, Z., Gattinoni, L., Yu, Z., Burns, W.R., Miermont, A.M., Teper, Y., Rudloff, U., et al. (2014). A novel chimeric antigen receptor against prostate stem cell antigen mediates tumor destruction in a humanized mouse model of pancreatic cancer. Hum. Gene Ther. *25*, 1003–1012.

38. Ramos, C.A., Rouce, R., Robertson, C.S., Reyna, A., Narala, N., Vyas, G., Mehta, B., Zhang, H., Dakhova, O., Carrum, G., et al. (2018). In vivo fate and activity of second- versus third-generation CD19-specific CAR-T cells in B cell non-Hodgkin's lymphomas. Mol. Ther. *26*, 2727–2737.

39. Pollok, K.E., Kim, Y.J., Zhou, Z., Hurtado, J., Kim, K.K., Pickard, R.T., and Kwon, B.S. (1993). Inducible T cell antigen 4-1BB. Analysis of expression and function. J. Immunol. *150*, 771–781.

40. Mardiana, S., John, L.B., Henderson, M.A., Slaney, C.Y., von Scheidt, B., Giuffrida, L., Davenport, A.J., Trapani, J.A., Neeson, P.J., Loi, S., et al. (2017). A multifunctional role for adjuvant anti-4-1BB therapy in augmenting antitumor response by chimeric antigen receptor T cells. Cancer Res. *77*, 1296–1309.

41. Wolfl, M., Kuball, J., Ho, W.Y., Nguyen, H., Manley, T.J., Bleakley, M., and Greenberg, P.D. (2007). Activation-induced expression of CD137 permits detection, isolation, and expansion of the full repertoire of $CD8^+$ T cells responding to antigen without requiring knowledge of epitope specificities. Blood *110*, 201–210.

42. Zhu, G., Flies, D.B., Tamada, K., Sun, Y., Rodriguez, M., Fu, Y.X., and Chen, L. (2001). Progressive depletion of peripheral B lymphocytes in 4-1BB (CD137) ligand/I-E_α)-transgenic mice. J. Immunol. *167*, 2671–2676.

43. Lee, S.W., Salek-Ardakani, S., Mittler, R.S., and Croft, M. (2009). Hypercostimulation through 4-1BB distorts homeostasis of immune cells. J. Immunol. *182*, 6753–6762.

44. Xu, Y., Zhang, M., Ramos, C.A., Durett, A., Liu, E., Dakhova, O., Liu, H., Creighton, C.J., Gee, A.P., Heslop, H.E., et al. (2014). Closely related T-memory stem cells correlate with in vivo expansion of CAR.CD19-T cells and are preserved by IL-7 and IL-15. Blood *123*, 3750–3759.

45. Connelly, J.P., and Pruett-Miller, S.M. (2019). CRIS.py: a versatile and high-throughput analysis program for CRISPR-based genome editing. Sci. Rep. *9*, 4194.

46. Ahmed, N., Salsman, V.S., Yvon, E., Louis, C.U., Perlaky, L., Wels, W.S., Dishop, M.K., Kleinerman, E.E., Pule, M., Rooney, C.M., et al. (2009). Immunotherapy for osteosarcoma: genetic modification of T cells overcomes low levels of tumor antigen expression. Mol. Ther. *17*, 1779–1787.

47. Kakarla, S., Chow, K.K., Mata, M., Shaffer, D.R., Song, X.T., Wu, M.F., Liu, H., Wang, L.L., Rowley, D.R., Pfizenmaier, K., and Gottschalk, S. (2013). Antitumor effects of chimeric receptor engineered human T cells directed to tumor stroma. Mol. Ther. *21*, 1611–1620.

48. Chow, K.K., Naik, S., Kakarla, S., Brawley, V.S., Shaffer, D.R., Yi, Z., Rainusso, N., Wu, M.F., Liu, H., Kew, Y., et al. (2013). T cells redirected to EphA2 for the immunotherapy of glioblastoma. Mol. Ther. *21*, 629–637.

49. Chan, W.K., Suwannasaen, D., Throm, R.E., Li, Y., Eldridge, P.W., Houston, J., Gray, J.T., Pui, C.H., and Leung, W. (2015). Chimeric antigen receptor-redirected CD45RA-negative T cells have potent antileukemia and pathogen memory response without graft-versus-host activity. Leukemia *29*, 387–395.

50. Cornetta, K., Duffy, L., Turtle, C.,J., Jensen, M., Forman, S., Binder-Scholl, G., Fry, T., Anne Chew, A., Maloney, D.G., and June, C.H. (2018). Absence of replication-competent lentivirus in the clinic: analysis of infused T cell products. Mol. Ther. *26*, 280–288.

51. Bauler, M., Roberts, J.K., Wu, C.-C., Fan, B., Ferrara, F., Yip, B.H., Diao, S., Kim, Y.I., Moore, J., Zhou, S., et al. (2019). Production of lentiviral vectors using suspension cells grown in serum-free media. Mol. Ther. Methods Clin. Dev. *17*, 58–68.

52. Cerignoli, F., Abassi, Y.A., Lamarche, B.J., Guenther, G., Santa Ana, D., Guimet, D., Zhang, W., Zhang, J., and Xi, B. (2018). In vitro immunotherapy potency assays using real-time cell analysis. PLoS ONE *13*, e0193498.